Fluorescent Superparamagnetic Core-Shell Nanostructures: Facile Synthesis of Fe@C-CN$_x$ Particles for Reusable Photocatalysts

Sankaran Murugesan, Oleksandr Kuznetsov, Zhou Zhou, Valery Khabashesku* [ID]

Center for Technology Innovation, Baker Hughes a GE Company, Houston, USA
Email: *valery.khabashesku@bakerhughes.com

Abstract

Synthesis and characterization of hybrid fluorescent superparamagnetic core-shell particles of Fe@C-CN$_x$ composition are presented for the first time. The prepared Fe@C-CN$_x$ hybrid nanoparticles were found to possess multifunctionality by exhibiting strong superparamagnetic properties and bright fluorescence emissions at 500 nm after the excitation with light in the UV-visible range. Fe@C-CN$_x$ also exhibits photocatalytic activities for organic dye degradation comparable to pure amorphous CN$_x$ with reusability through magnetic separation. The combination of magnetic and fluorescent properties of core-shell Fe@C-CN$_x$ nanoparticles opens opportunities for their application as sensors and magnet manipulated reusable photocatalysts. Superparamagnetic Fe@C core-shell nanoparticles were used as the template material in the synthesis, where the carbon shell was functionalized through one-step free-radical addition of alkyl groups terminated with carboxylic acid moieties. The method utilizes the organic acyl peroxide of dicarboxylic acid (succinic acid peroxide) as a non-oxidant functional free radical precursor for functionalization. Further, covalently functionalized succinyl-Fe@C core-shell nanoparticles were coated with the amorphous carbon nitride (CN$_x$) generated by an *in-situ* solution-based chemical reaction of cyanuric chloride with lithium nitride. A detailed physicochemical characterization of the microstructure, magnetic and fluorescence properties of the synthesized hybrid nanoparticles is provided.

Keywords

Magnetic Nanoparticles, Core-Shell Nanostructures, Fe@C-CN$_x$, Fluorescence, Photocatalysts

1. Introduction

Magnetic nanoparticles create tremendous interests largely because of their

unique properties towards biomedical applications for cancer treatment that combine a targeted drug delivery and hyperthermia [1] [2] [3]. Superparamagnetic iron oxide nanoparticles (SPIONs) in the form of magnetite (Fe_3O_4) and maghemite (γ-Fe_2O_3) have been commonly used for this purpose [4] [5]. Magnetic properties of these materials are strongly influenced by colloidal dispersion and particle size. In order to stabilize these particles in colloidal systems, a suitable polymer attachment/loading or chemical treatment has been implemented. However, with the increase in loading of polymers, the activity of SPIONs decreases. Moreover, SPIONs are also susceptible to the change in pH and ion concentration in biological fluids.

Alternative materials having higher superparamagnetic properties, such as iron carbides and carbon-coated Fe, were recently explored [6] [7] [8] [9]. For example, the carbon coated Fe nanoparticles, Fe@C, which exhibit strong superparamagnetic properties, have been used as MRI contrast enhancement agents [10]. The presence of carbon shell in the core-shell nanostructures is very important since such shell acts as a protective coating to magnetic cores against chemical components of biological fluids and is inert to pH changes. The carbon shell also facilitates the particles to be stable to chemical environments and treatment procedures. The presence of carbon shell provides opportunities to introduce functional groups on the carbon surface. A series of methods for functionalization of carbon materials and carbon based nanoparticles have been developed. These methods involve either non-covalent functionalization by physical adsorption of chemical compounds, such as polymers, or oxidative route to covalently introduce functional groups. The oxidative functionalization process is however accompanied by oxidation of Fe core in Fe@C particles and decrease of superparamagnetic properties. Strong chemical interaction between the surface carbon network and the functional groups through a covalent carbon-carbon bonding is preferred. Different functional groups, e.g., amino, hydroxyl, alkyne, or maleimido groups, have been covalently bonded to Fe@C nanoparticles through a two-step reaction with aryl diazonium salts [6]. This process is nevertheless limited to bonding only the aryl moieties to carbon shell surface of nanoparticles. Continuing search for simple efficient methods to introduce organic functional groups capable of further modification tailoring the nanoparticle properties towards specific applications is an active field of research. In this work, a mild organic reaction based on succinic acid peroxide was used to generate and covalently attach carboxyl terminated free alkyl radicals as functional groups to the carbon shell of Fe@C nanoparticles. This technique has previously been effectively applied for a non-destructive to the side walls functionalization of carbon nanotubes [11].

For specific applications, engineering of multifunctional properties in the nanoparticles is particularly desirable. For example, multi-functionality can be introduced by combination of at least two different physico-chemical properties such as optical (fluorescence) and magnetic. This approach has been explored in

the biomedical multitasking applications like sensing and manipulations [12]. For imaging of magnetic nanoparticles in biological systems, a suitable dyes or chemical compounds have been widely used as additives. However, possession of fluorescence properties by the same magnetic particles can eliminate the need of addition of organic fluorophores (dyes) required for biological imaging. To realize this idea, an approach based on creation of different coating shells over superparamagnetic metal and metal oxide nanoparticles to produce hybrid materials can be taken.

Among a potential selection of coating materials, CN_x presents an interesting choice since it shows a mix of attractive photophysical and catalytic properties. Recently, this material has been exploited for very challenging catalytic reactions and photochemical water splitting as well as metal free electrochemical oxygen reduction [13]. Generally, CN_x has been synthesized through thermal decomposition of melamine and hydrothermal process. Although in these processes it is difficult to control the morphology and nanostructure, some attempts were made to coat CN_x over different particles to harvest hybrid properties. One such example involved a coating of CN_x over several carbon nanomaterials (diamond, graphene, graphene oxide) for improved catalytic performance [14]. Earlier reported efforts have been successful in developing a low temperature solution based synthesis of sphere-shaped CN_x of C_3N_4 stoichiometry [15] [16]. This spherical onion-like CN_x shows higher light emission quantum yield than graphitic CN_x [17] [18]. The enhanced fluorescence intensity in spherical C_3N_4 is due to the anti-Stokes fluorescence property. The demonstrated method of wet chemical synthesis [15] appears to be suitable for coating CN_x over different colloidal particles. It has particularly been shown that C_3N_4 can be coated over colloidal silica spherical nanoparticles [15] [16].

In this study, we report for the first time the synthesis of core-shell superparamagnetic iron nanoparticles coated with the fluorescent sphere-shaped CN_x shells. This was performed through a two-step chemical procedure. The existence of thick carbon shell around the superparamagnetic iron core played an important role in the surface functionalization. Further, the covalently attached functional groups acted as anchoring sites for the CN_x spheres which have been *in-situ* synthesized and coated over core-shell Fe@C nanoparticles. The synthesized hybrid Fe@C-CN_x nanoparticles have been characterized by different analytical techniques and fluorescence properties were studied.

2. Materials and Methods

2.1. Synthesis of Succinic Acid Peroxide

To prepare succinic acid acyl peroxide an earlier reported procedure has been adopted [11]. Briefly, 10 g of succinic anhydride fine powder (Aldrich) was added to 20 mL of ice cold 8% hydrogen peroxide and stirred for 30 min until all of the powder dissolved and a white gel like solution formed. The solution was filtered onto a 1-μm pore size PTFE membrane (Cole Palmer) to leave a deposit

which was washed with a small amount of water and then air-dried for 10 min. The white peroxide product has been transferred from the membrane to a glass vial and vacuum-dried at room temperature for 24 h.

2.2. Functionalization of Fe@C

20 mg of Fe@C black powder (Sigma Aldrich) was placed in 200 mL of dry o-dichlorobenzene and sonicated for 30 min. Then the mixture was heated in a N_2 atmosphere at 110°C for 2 days with the periodic addition of 2.5 g total of succinic acid peroxide. After reaction completion, the product was washed by pouring large quantity of chloroform and sonication for 30 min, and then filtered. The final product, succinyl functionalized Fe@C, was washed multiple times with THF and ethanol.

2.3. Synthesis of Core-Shell Fe@C-CN$_x$ Particles

For this purpose, *in-situ* formation of CN$_x$ through the reaction of cyanuric chloride with lithium nitride [15] in the presence of succinyl functionalized Fe@C as the core template, providing through the terminal carboxyl groups the ancoring sites for the CN$_x$ spherical nanoparticles, has been adopted. Lithium nitride (5.2 mmol) and cyanuric chloride (10.4 mmol) in 150 ml of dry diglyme were placed in round bottom flask and refluxed under nitrogen atmosphere for 24h (Scheme 1). Reactions were done with and without adding a succinyl functionalized Fe@C. The formed slowly precipitating yellow powder was filtered of diglyme, washed with ethanol and water, and then dried in vacuum oven. The powder obtained with succinyl functionalized Fe@C was again re-dispersed in water and then magnetically active material has been separated from a non-magnetic CN$_x$ by-product by using a strong magnet.

Further, this material has been separated into two differently colored materials: a black colored one with the use of strong magnet and another one green in color with weak magnetic separation. Both materials were characterized and compared with the amorphous CN$_x$ (pure a-CN$_x$), a yellow powder prepared without Fe@C particles.

2.4. Photocatalytic Experiments

Rhodamine B (*N,N,N',N'*-tetraethylrodamine) (RhB) was used as the model dye
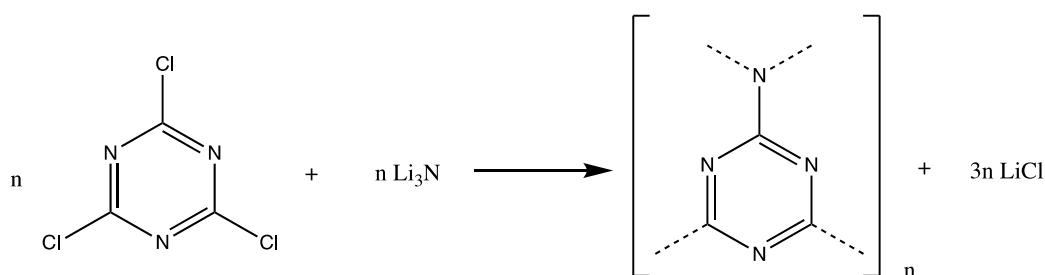
Scheme 1. Synthesis of amorphous CN$_x$ [15] [16].

compound for testing the catalytic activity of Fe@C-CN$_x$ particles in photooxidation reactions. Reactions were performed with 10 mg of test sample placed in 50 mL of organic dye solution. Before shining the light, solution was allowed to stir for 30 min to obtain the equilibration between adsorption-desorption of dye and photocatalyst. The solution was exposed to 365 nm Pen Ray UV-light with the intensity of 145 μW/cm² under constant magnetic stirring. The test samples were withdrawn from the reaction mixture at regular intervals and filtered through a 0.2 μm PTFE membrane filter to remove photocatalyst. The absorption spectra of filtrates were measured using a UV-Vis spectrometer. Initial peak intensity of the RhB at 554 nm directly proportional to the concentration was taken as C$_o$ and the change in the concentration of RhB (C) was monitored by measuring the declining intensity of the same peak in the course of reaction. The ratio of C/Co with respect to irradiation time was used for evaluation of the efficiency of the photocatalyst.

2.5. Materials Characterization

The occurrence of chemical functionalization of nanoparticles was confirmed by presence of characteristic signatures in the infrared spectral region. The FTIR spectra were obtained in ATR mode using Thermo Fisher instrument equipped with the diamond ATR accessory. The ATR FTIR spectra of the samples placed over the diamond crystal surface were collected at 64 scans with 4 cm⁻¹ resolution. The changes in crystallinity of Fe@C materials after the functionalization were analyzed from X-ray powder diffraction patterns obtained with a Rigaku D/Max Ultima II Model instrument equipped with a Cu Kα radiation source operating at 40 kV and 40 mA. Thermogravimetric analysis (TGA) experiments were performed using a TA Q500 instrument with Nitrogen as a purge gas at a flow rate of 40 mL/min at heating rate of 10˚C /min up to 900˚C. The change in weight with temperature was plotted.

The morphology of functionalized and CN$_x$ coated Fe@C samples has been analyzed by Scanning Electron Microscopy (SEM) using a JEOL field emission scanning electron microscope JSM-7800. EDS elemental analysis was performed at 15 kV with working distance of 10 mm to determine the relative ratios of iron, oxygen, carbon, and nitrogen present on the as-received, functionalized and CN$_x$ coated Fe@C. The superparamagnetic properties of the Fe@C, before and after the functionalization and coating with CN$_x$, were measured with the Quantum Design MPMS SQUID System. The measurements were performed in dynamic mode up to 5 Tesla with opposite polarity. All measurements were done at 300 Kelvin.

X-ray photoelectron spectroscopy (XPS) data were collected on a Physical Electronics PHI 7500 XPS spectrometer with an Al Kα radiation source (1486.6 eV), at power setting of 350 W and an analyzer pass energy of 23.5 eV. Fluorescence measurements were carried out using a Horiba Jobin Yvon Fluorolog 3 spectrofluorometer equipped with a single grating monochromator and a pho-

tomultiplier tube detector having an accuracy of 0.5 nm. Optical absorption spectral data were collected on a Shimadzu UV-3600 UV-VIS-NIR spectrophotometer equipped with the integrating sphere for diffuse reflectance measurements. The samples were prepared on a glass slide with the silicone grease. Light from the spectrophotometer grating was incident normally to the sample surface. The measurement scans were performed in the 300 - 800 nm spectral range.

3. Results and Discussion

Scheme 2 represents the overall process of synthesis of Fe@C-CN$_x$ core-shell nanoparticles. Spherical CN$_x$ was coated over a carbon shell covered magnetic Fe nanoparticles. Initially, the surface of the carbon shell on the Fe core was functionalized with the succinyl moieties terminated with the carboxylic groups. The latter served as anchors for grafting and coating the in situ generated CN$_x$ onto the Fe@C surface as well as enable better dispersion of the Fe@C particles in the reaction media (diglyme).

ATR-FTIR spectra of Fe@C, succinyl functionalized Fe@C, and CN$_x$ coated succinyl functionalized Fe@C particles are compared in **Figure 1**. The spectrum of Fe@C powder does not show any features while spectrum of succinyl functionalized Fe@C nanoparticles shows a broad band in the 3000 - 3500 cm^{-1} region related to the O-H stretches and weak bands of the C-H stretches in the 2800 to 3000 cm^{-1} range. Absorption peak near 1740 cm^{-1} is characteristic of the carbonyl group (**Figure 1(b)**). Presence of these peaks in the spectrum of succinyl functionalized Fe@C (**Figure 1(b)**) confirms the functionalization process. Our results are consistent with the earlier report on a non-oxidative functionalization of carbon nanotube sidewalls when they are reacting with the succinic acid peroxide [11]. More commonly used oxidative functionalization process on Fe@C particles tends to oxidize not only the carbon shell but also the metal core [7]. On the contrary, the current method of utilizing the succinic acid peroxide seems to be nondestructive to the carbon shell surface keeping the Fe core mainly intact. The functionalized Fe@C nanoparticles have been surface coated with the CN$_x$ to harvest the additional benefit of thus produced hybrid particles. Graphitic CN$_x$ materials prepared by different methods are known to show fluorescence properties. CN$_x$, of spherical morphology, prepared through chemical reaction of cyanuric chloride with lithium nitride in diglyme medium, exhibits higher quantum efficiency of the fluorescence than graphitic CN$_x$ synthesized by high temperature (460°C - 650°C) reactions [19]. FTIR spectrum of Fe@C-CN$_x$
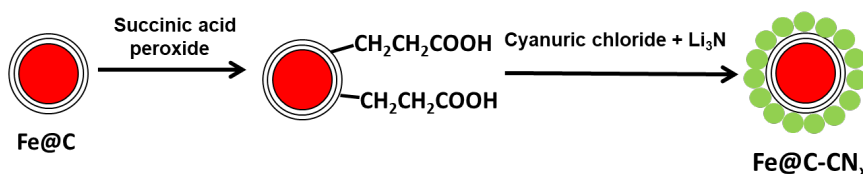
Scheme 2. Two-step process for synthesis of hybrid nanoparticles.
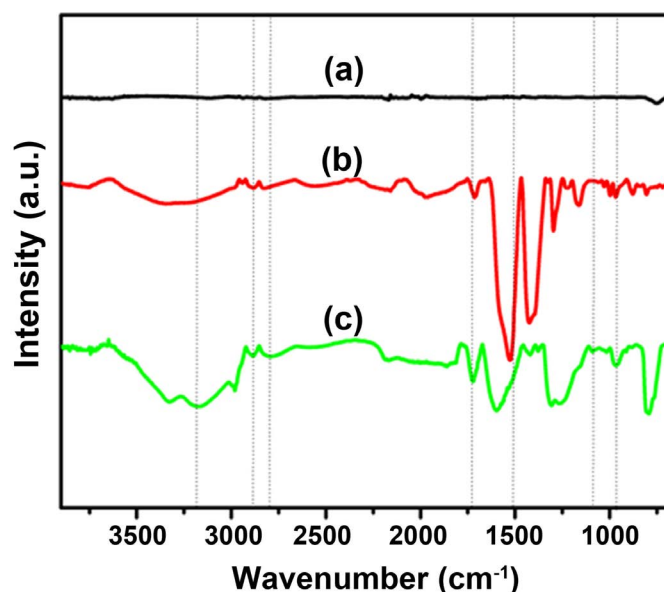
Figure 1. ATR-FTIR spectra of (a) Fe@C, (b) succinyl functionalized Fe@C, and (c) succinyl functionalized Fe@C particles coated by CN_x and separated from the reaction mixture by magnet.

(Figure 1(c)) shows the presence of bands at 807, 1440, and 1490 cm^{-1} which belong to s-triazine ring modes, while the peaks in the 1000 - 1350 cm^{-1} region belong to the C-N stretching modes. Also, broad bands of stretching modes of the NH and NH_2 (and possibly OH) groups at 3342 cm^{-1} and a weak band at 2177 cm^{-1} due to the C≡N group are present. The spectrum shown on Figure 1 also exhibits two weak bands in the 2800 - 3000 cm^{-1} region and a stronger bands at 1250 and 1735 cm^{-1} which belong to the CH_2, C-O and C=O stretching modes, respectively, of the succinyl groups in the CN_x coated succinyl functionalized Fe@C.

X-Ray powder diffractometry was performed to find out if any changes in the oxidation state of Fe core in Fe@C particles took place during the functionalization. Figure 2 shows the XRD patterns of the as-received Fe@C and functionalized Fe@C powders in comparison with the reference peaks of iron and its oxides. The analysis of the as-received powder shows the presence of bccFe (110) and Fe_3C (211) peaks in the 42 - 44 2-theta region. The peak of Fe_3C remains intact while no other prominent peaks appear in the XRD of Fe@C after the functionalization (Figure 2(a)). These data mean that no significant destruction of carbon shells in the as-received Fe@C powder occurs during the treatment with succinic acid peroxide.

SEM imaging (Figure 3(a)) and EDS analysis show that the as-received Fe@C powder is polydispersed with the particle sizes ranging from 20 to 100 nm, and the bulk content of carbon in the core-shell particles is about 19%. After treatment with the succinic acid peroxide and functionalization with the succinyl moieties, the carbon and oxygen contents increased from 19 to 26 wt% for carbon, and from 3.3 to 6.5 wt% for oxygen. These data provide further evidence
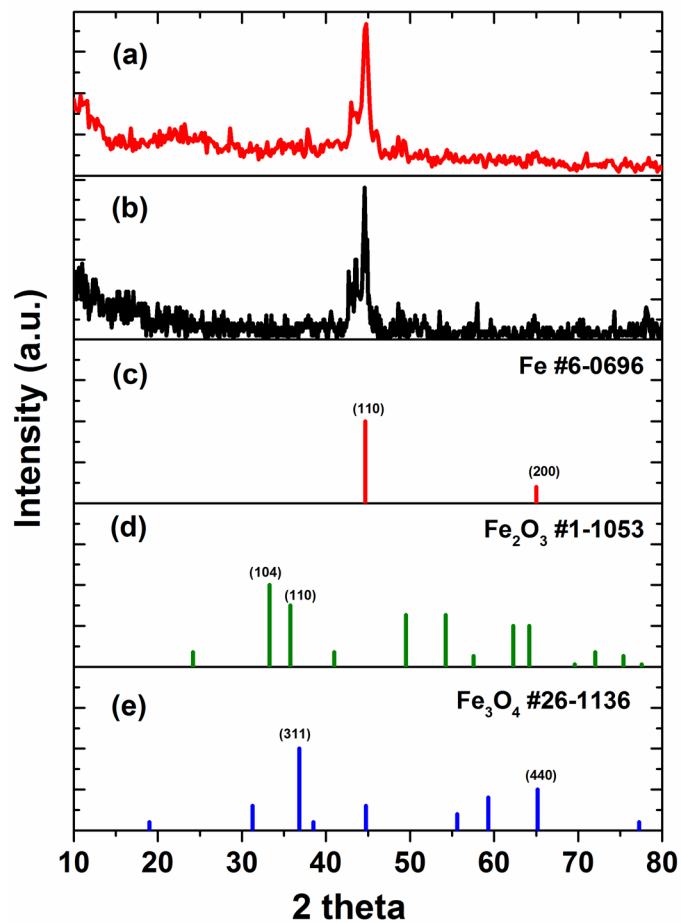
Figure 2. XRD patterns of functionalized Fe@C (a), as-received Fe@C (b), pure metallic Fe powder (JCPDS#6-0696) (c), Fe₂O₃ (JCPDS#1-1053) (d), and Fe₃O₄ (JCPDS#26-1136) (e).
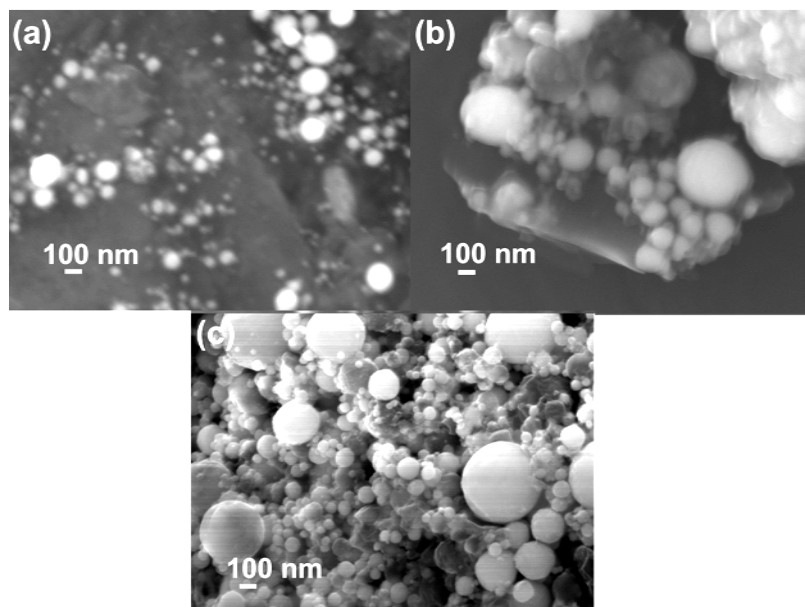
Figure 3. SEM images of as-received Fe@C (a), succinyl functionalized Fe@C (b), and CN_x coated succinyl functionalized Fe@C (c).

for the functionalization of Fe@C nanoparticles. Analysis of CN_x coated succinyl functionalized Fe@C particles, both black and green colored, showed the presence of nitrogen in the sample. The magnetic particles containing low Fe concentration in the core appear green colored which suggests that Fe@C particles become covered with thick clusters of spherical CN_x. These green CN_x coated Fe@C particles were used for further studies.

The amount (wt%) of organic functional groups on the surface of Fe@C particles was estimated from the TGA data obtained in the experiments run under nitrogen atmosphere. Figure 4 presents the TGA plots obtained for Fe@C, succinyl functionalized Fe@C, pure a-CN_x and CN_x coated succinyl functionalized Fe@C (green) samples. Figure 4(a) for Fe@C shows very low total weight loss (less than 7 wt%) at 900°C most likely due to the degradation of the part of carbon shell, containing an incorporated oxygen, which results in elimination of CO_2. In comparison, the degradation in the functionalized Fe@C facilitate a total weight loss of about 40% at 900°C (Figure 4(b)) with the contribution of ~20 wt% from the degradation of succinyl moieties in the 200°C - 500°C temperature range. Figure 4(c) shows the thermal decomposition of amorphous pure-CN_x which undergoes 100% weight loss at 900°C in agreement with previous data [15] [16]. In comparison, Figure 4(d) shows that the thick CN_x coated over the succinyl functionalized Fe@C produces a residue of 5 wt% at 900°C, which is due to the presence of Fe core.

TEM images (Figure 5) show both the presence of thick graphitic shell over the Fe core in Fe@C nanoparticles and that this core is mainly preserved after the functionalization reaction. Also, some carbon deposit over the surface of the particle is observed as the result of thermal decomposition of succinic acid peroxide used for functionalization. The products of decomposition of succinic
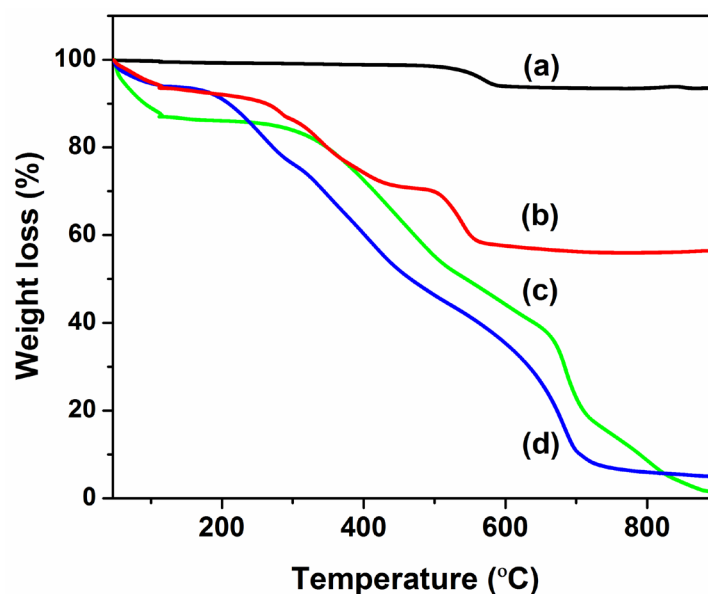
Figure 4. TGA plots for Fe@C (a), functionalized Fe@C (b), pure a-CN_x (c), and CN_x coated functionalized Fe@C (d).
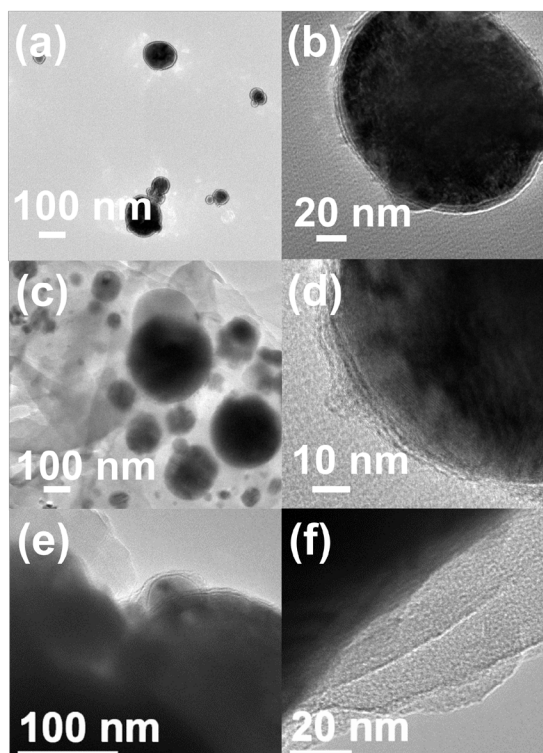
Figure 5. TEM images of as-received Fe@C (a) (b) and succinyl functionalized Fe@C (c) (d) nanoparticles, and CN_x coated succinyl functionalized Fe@C at low (e) and high (f) magnification showing coating.

acid peroxide form additional carbon layers around the magnetic Fe@C particles. These carbon layers contain the covalently attached succinyl moieties which seem to be of too small size for direct imaging. The thicknesses of the particles thus become increased due to the functionalization. This confirms that the undertaken functionalization process is a mild and efficient way to introduce the functional groups over the Fe@C carbon shell compared to other methods documented in the literature. In more detail, analysis by TEM (Figure 5(e); Figure 5(f)) confirms the presence of extra thick coating layers around the Fe@C as the constituents of the hybrid structure of Fe@C-CN_x.

Comparison of the XPS survey spectra of succinyl functionalized Fe@C and CN_x coated Fe@C shown in Figure 6(a) (plots i and ii) provide evidence for the fact that the coating has been added to the surface of functionalized Fe@C particles and it is mainly composed of carbon and nitrogen. High resolution XPS data for C1s peak and N1s peaks are presented in deconvoluted mode on Figure 6(b) and Figure 6(c), respectively. The curve fit contributions into a C1s peak at 283.8, 285.1, and 287.3 eV (Figure 6(b)) were attributed to the C-C, C-O, and C=N bonds, respectively. The deconvoluted N1s peak (Figure 6(c)) shows a major peak at 397.7 eV due to the sp^2 nitrogens bonded to carbon within the triazine rings, and a shoulder peak at higher binding energy, 398.9 eV, assigned to a 3-coordinated nitrogens, each bridging three triazine rings in the CN_x structure [15] [16]. The arc produced Fe@C particles, used as templates in our work,
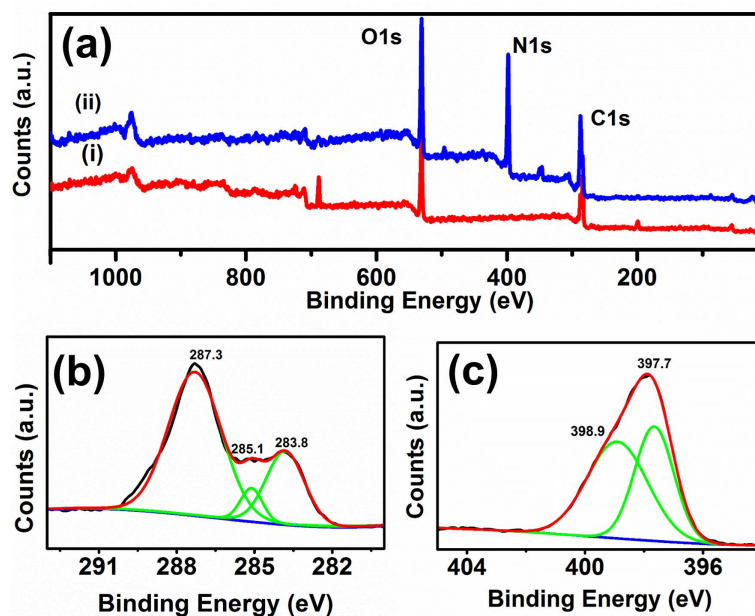
Figure 6. (a) XPS survey spectra of succinyl functionalized Fe@C (i) and Fe@C-CN$_x$ (ii), high resolution XPS data for C1s (b), and N1s (c) peaks for Fe@C-CN$_x$.

were reported [20] to have the thickness of carbon coatings of 4 - 5 nm. Such carbon shell, especially after the overcoating with thick CN$_x$ layers, has virtually precluded the detection of Fe by XPS which as a surface analysis technique has a typical analysis depth of less than 5 nm.

Magnetic measurements for these core-shell particles were performed at 300 K using SQUID instrument. **Figure 7** presents magnetization curves (M vs. H) obtained for the as-received Fe@C nanopowder, and succinyl functionalized Fe@C and Fe@C-CN$_x$ products. The curves show typical superparamagnetic behavior for all studied materials, characterized by the absence of the magnetic hysteresis loop. Magnetic moments are corrected with respect to weight percent of Fe content obtained from TGA analysis (**Figure 4**). The analysis shows that magnetic moment (emu/g) of tested powders decreases after the functionalization from 130 emu/g in Fe@C to 95 emu/g in succinyl functionalized Fe@C and 75 emu/g in Fe@C-CN$_x$. This can be related to the increasing content of a non-magnetic coating added over the magnetic core in the core-shell nanoparticles of Fe@C (magnetization curve **a**) after their conversion first into a succinyl functionalized derivative (curve **b**) followed by overcoating with the CN$_x$ to form a Fe@C-CN$_x$ product (curve **c**). The synthesized Fe@C-CN$_x$ particles show strong magnetic behavior which allowed their separation by the lab magnet from the solution of reaction mixture containing a non-magnetic CN$_x$ particles formed as a by-product.

To understand the optical properties of pure a-CN$_x$ and Fe@C-CN$_x$ particles, diffuse reflectance (DR) UV-Vis spectra were measured (**Figure 8**). All the measurements were compared with TiO$_2$ as a model compound. From the UV-Vis DR spectra showing strong cut off for TiO$_2$ at 408 nm (**Figure 8(a)**), the band gap has been calculated by the following procedure:
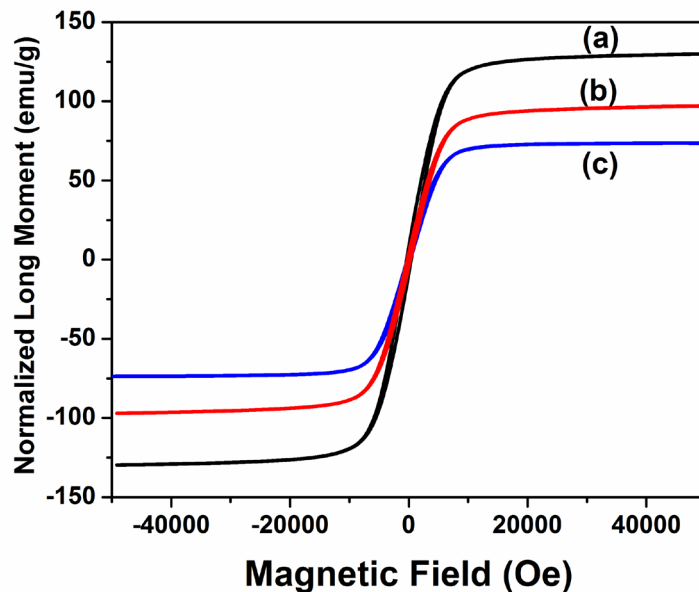
Figure 7. The curves of magnetization versus the applied field obtained by SQUID at room temperature for as-received Fe@C (a), succinyl functionalized Fe@C (b), and Fe@C-CN$_x$ (c).
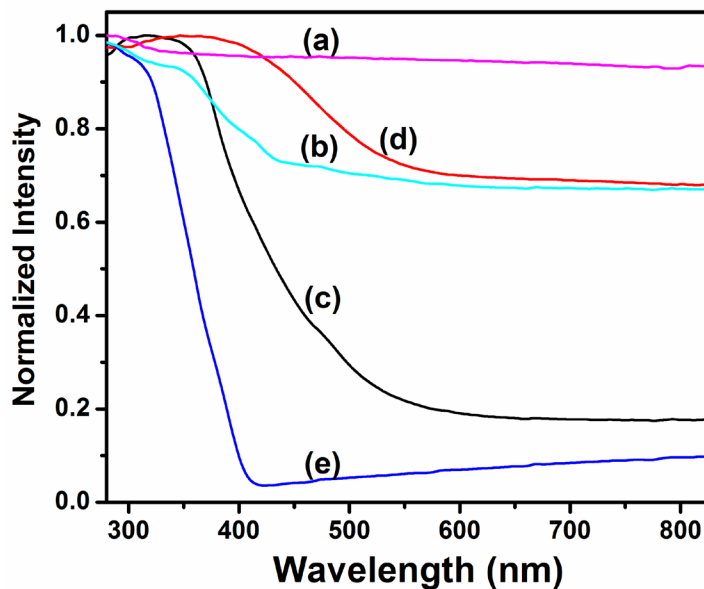
Figure 8. Comparison of the diffuse reflectance (DR) UV-Vis spectra of Fe@C (a), functionalized Fe@C (b), pure a-CN$_x$ (c), CN$_x$ coated over functionalized Fe@C (d), and commercial TiO$_2$ (Sigma Aldrich, 20 nm) (e) powders.

$$\text{Band Gap Energy (E)} = h \times C/\lambda$$

$$h = \text{plank constant} = 6.626 \times 10^{-34} \text{ Joules sec}$$

$$C = \text{Speed of light} = 3.0 \times 10^8 \text{ meter/sec}$$

$$\Lambda = \text{Cut of wavelength} = 408 \times 10^{-9} \text{ meters}$$

where 1 eV = 1.6×10^{-19} Joules (conversion factor).

Similarly, calculated band gap values for a-CN$_x$ and Fe@C-CN$_x$ particles are shown in Table 1.

TiO$_2$ shows band edge of 408 nm with a bandgap of 3.0 eV; this is lower than the theoretical band gap value of TiO$_2$ (3.2 eV). This may be due to the particle size effect (TiO$_2$ particle size 20 nm). Pure a-CN$_x$ (Figure 8(b)) showed red shift in the absorption band edge at 488 nm with the band gap of 2.6 eV. Fe@C-CN$_x$ particles (Figure 8(c)) also showed red shift compared to TiO$_2$ and pure a-CN$_x$ with the band edge of 552 nm and band gap as low as 2.3 eV which is likely due to electron doping from conducting graphene underlayers to CN$_x$ semiconducting outer layers It is also noticed that the absorption in the visible region shifts the baseline higher. This may be due to presence of carbon shell over the Fe core which makes the CN$_x$ coated over succinyl functionalized Fe@C to show a green color. The picture given in Figure 9 shows a color difference between the TiO$_2$ (a), pure a-CN$_x$ (b) and Fe@C-CN$_x$ (c) particles.

This hybrid Fe@C-CN$_x$ structure was studied for fluorescence activity in a solid state mode with a right angle measurements. It was shown earlier that the spherical CN$_x$ exhibits enhanced fluorescence activity compared to the graphitic CN$_x$ which is possibly due to the resonance scattering of laser light by spherical particles [18]. In this paper, the fluorescence property of a core-shell hybrid system has been compared with the pure a-CN$_x$. Figure 10(a) presents the fluorescence spectra of pure a-CN$_x$ spherical particles showing a strong fluorescence signal with maximum emission at 460 - 470 nm with the emission peak position being very low dependent of variable excitation wavelengths (335, 350, 365 and 380 nm). It also showed a sharp excitation at 350 nm that was measured by using the emission wavelength of 460 nm (Figure 10(b)). In comparison, the Fe@C-CN$_x$ hybrid system showed a red shift of the emission peak at 500 nm obtained with different excitation wavelengths (335, 350, 365 and 380 nm) (Figure 10(c)). It showed a strong excitation at 365 nm determined with the emission wavelength set at 500 nm (Figure 10(d)). Three dimensional plots of fluorescence property with excitation and emission wavelengths for pure a-CN$_x$ and Fe@C-CN$_x$ are given in Figure 11(a) and Figure 11(b). The red shift in the emission detected for Fe@C-CN$_x$ relatively to pure a-CN$_x$ may be attributed to the influential effect of electromagnetic spectrum on magnetic Fe core in the hybrid configuration. In addition, the red shift in the fluorescence may be also attributed to a thin graphene-like carbon layer over Fe core and interaction with the CN$_x$ coating in the Fe@C-CN$_x$ core-shell nanoparticles [21] [22].

Table 1. Absorption band edges and calculated band gap values for TiO$_2$, a-CN$_x$ and Fe@C-CN$_x$ particles.

Compound	Absorption edge (nm)	Band gap energy (E$_g$, eV)
TiO$_2$	408	3.0
a-CN$_x$	488	2.6
Fe@C-CN$_x$	552	2.3
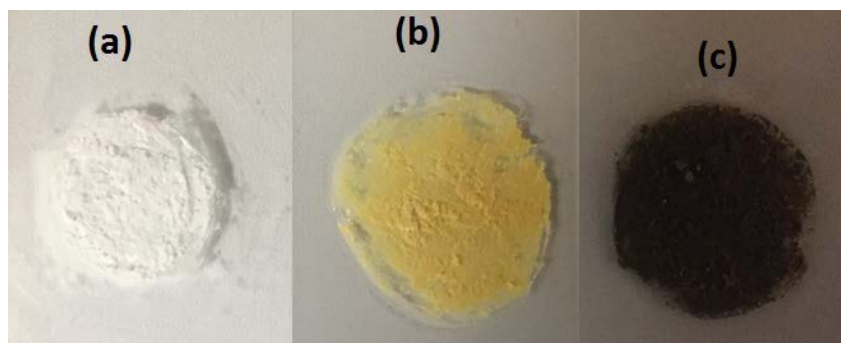
Figure 9. The picture shows a color difference between the TiO_2 (a), pure a-CN_x (b) and Fe@C-CN_x (c) particles.
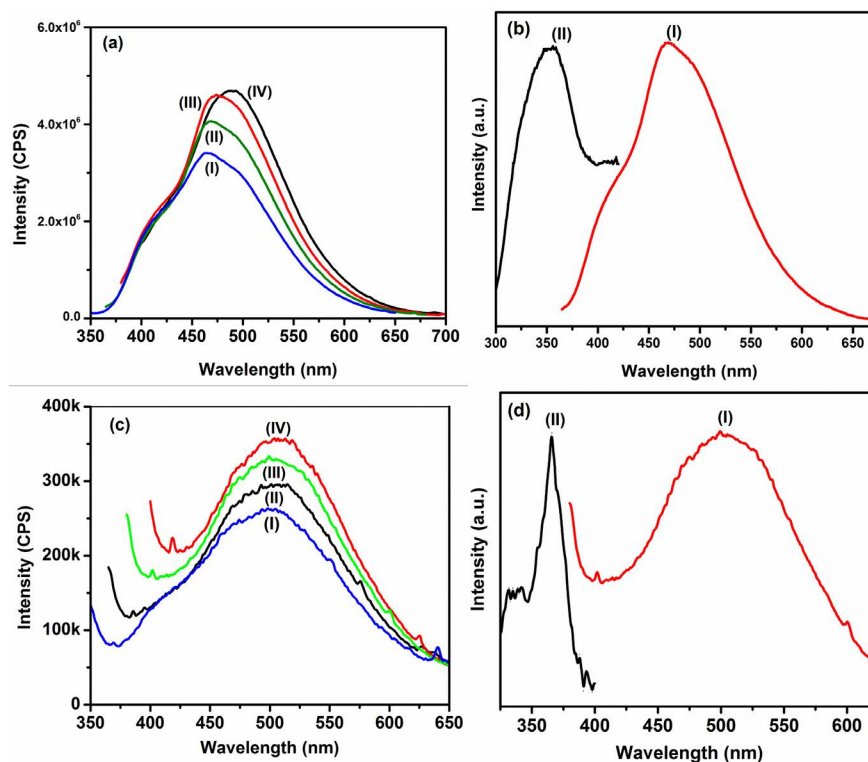
Figure 10. Emission spectra for pure a-CN_x obtained with the excitation at different wavelength [(I) 335 nm, (II) 350 nm, (III) 365 nm and (IV) 380 nm] (a). Excitation and emission spectra of spherical CN_x with the maxima at 350 nm (II) and 470 nm (I), respectively (b). Emission spectra of Fe@C-CN_x particles obtained with the excitation at different wavelengths [(I) 335 nm, (II) 350 nm, (III) 365 nm and (IV) 380 nm] (c). Excitation and emission spectra of Fe@C-CN_x particles with the maxima at 365 nm (II) and 500 nm (I), respectively (d).

The photocatalytic performance of the Fe@C-CN_x was examined and compared with pure CN_x by monitoring the degradation of RhB (**Figure 12**). This organic dye is known to be stable towards self-degradation under illumination and also not degrade in presence of photocatalyst in absence of illumination [23]. The amount of photocatalyst constituent in Fe@C-CN_x was calculated from the TGA results on weightloss difference between pure Fe@C, succinyl functionalized
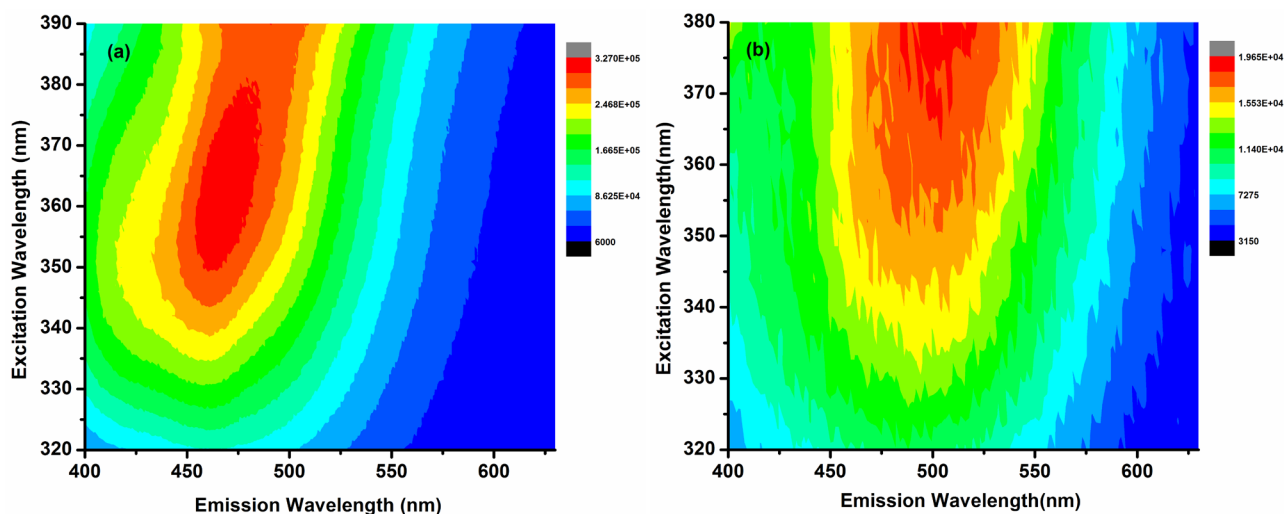
Figure 11. 3D-excitation and emission profile of a-CN$_x$ (a) and Fe@C-CN$_x$ (b) showing the red shift in the emission properties.
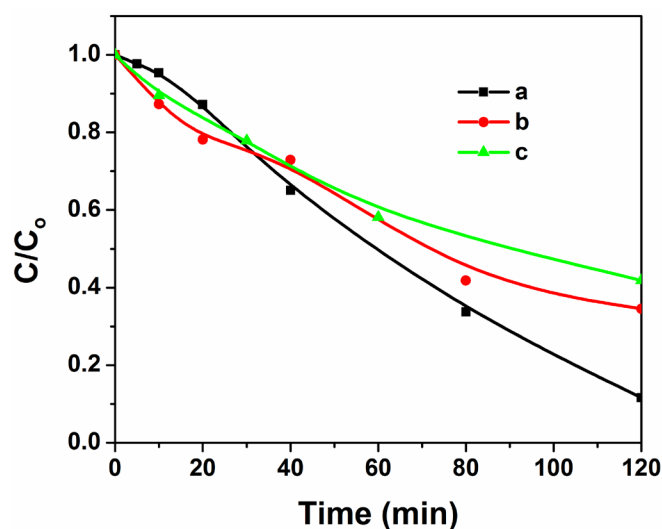
Figure 12. Photocatalytic degradation curves for Rhodamine B obtained in the presence of pure CN$_x$ (a), Fe@C-CN$_x$ (b), and reused Fe@C-CN$_x$ (c) at different time intervals. Change in the concentration (C/C$_o$) of RhB was calculated from the decreasing absorption peak intensity at 554 nm.

Fe@C and Fe@C-CN$_x$ samples. The RhB dye shows a strong absorption band around 554 nm (**Figure 13**).

Photodegradation of RhB under 365 nm illumination for 120 min is at about 88% in the presence of pure CN$_x$ (**Figure 12(a)**) and 65% for Fe@C-CN$_x$ (**Figure 12(b)**). Some difference in the photocatalytic activity may be attributed to the choice of light source for the illumination and to different amount of active sites on the surface of pure and core-shell nanoparticles.

The advantage of coating the photoactive materials over magnetic particles comes with the possibility of reusability. **Figure 14** shows the photograph of Fe@C-CN$_x$ particles separated from the reaction media by the magnet. The reusability can provide for unique applications of the photocatalyst. Indeed, the
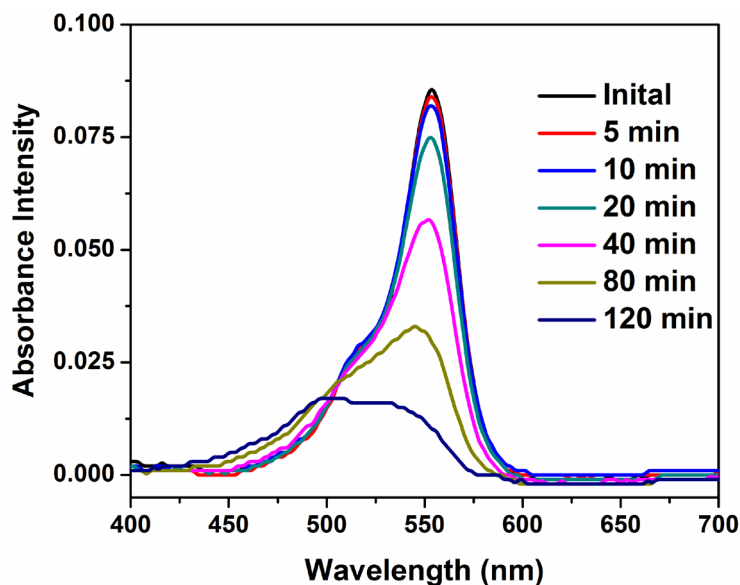
Figure 13. Absorption spectra indicating the photocatalytic decomposition of Rhodamine B by Fe@C-CN$_x$ under illumination with 365 nm of 0.16 mW light source measured at different time intervals.

Figure 14. Fe@C-CN$_x$ dispersed in the reaction medium and magnetically separated after the photocatalytic reaction.

reused Fe@C-CN$_x$ particles were shown to enable the similar degradation of RhB dye at as a high yield as 58% (**Figure 12(c)**). However, the dye degradation results show that besides the yield there is also a difference in kinetics between pure CN$_x$ and Fe@C-CN$_x$ which may be attributed to the porosity and the surface area of the samples. Further the interaction of amorphous CN$_x$ with thin carbon shell over superparamagnetic Fe core enable better charge separation efficiency and photocatalytic activity in redox reaction [24] [25].

4. Conclusion

In summary, a facile chemical method for synthesis of hybrid fluorescent magnetic core-shell particles has been described. This method applies an especially mild technique to covalent organic functionalization of thick carbon shells over the core of superparamagnetic Fe@C nanoparticles followed by their *in-situ* generated coating of spherical CN_x. The synthesized Fe@C-CN_x hybrid nanoparticles possess multifunctionality by exhibiting strong superparamagnetic properties and bright fluorescence emissions at 500 nm after the excitation with light in the UV-visible range. In view of the ongoing research on applications of CN_x in photocatalytical systems [26] [27] [28] [29] [30] and after taking into account the combination of magnetic and fluorescent properties of core-shell Fe@C-CN_x nanoparticles, one can propose his application for a design of photocatalysts that can be separated and removed by magnets from a liquid reaction system and then can become potentially reusable, as the preliminary results of this work have shown that. Besides, the synthetic method described herein presents a new opportunity for preparation of not only a Fe@C based but also other magnetic metal core-fluorescent CN_x shell compounds. Creation of these hybrid nanostructures makes these compounds unique for different applications utilizing both magnetic and fluorescence properties enabling their particular use in sensing [31], actuation and particles' manipulation.

Conflicts of Interest

The authors declare no conflicts of interest.

References

[1] Jordan, A., Scholz, R., Wust, P., Fakhling, H. and Felix. R. (1999) Magnetic Fluid Hyperthermia (MFH): Cancer Treatment with AC Magnetic Field Induced Excitation of Biocompatible Superparamagnetic Nanoparticles. *Journal of Magnetism and Magnetic Materials*, **201**, 413-419. https://doi.org/10.1016/S0304-8853(99)00088-8

[2] Duerr, S., Janko, C., Lyer, S., Tripal, P., Schwarz, M., Zaloga, J., Tietze, R. and Alexiou, C. (2013) Magnetic Nanoparticles for Cancer Therapy. *Nanotechnology Reviews*, **2**, 395-409. https://doi.org/10.1515/ntrev-2013-0011

[3] Revia, R.A. and Zhang, M. (2016) Magnetite Nanoparticles for Cancer Diagnosis, Treatment, and Treatment Monitoring: Recent Advances. *Materials Today*, **19**, 157-168. https://doi.org/10.1016/j.mattod.2015.08.022

[4] Rana, S., Jadhav, N.V., Barick, K.C., Pandeyb, B.N. and Hassan, P.A. (2014) Polyaniline Shell Cross-Linked Fe_3O_4 Magnetic Nanoparticles for Heat Activated Killing of Cancer Cells. *Dalton Transactions*, **43**, 12263-12271.

[5] Devkota, J., Mai, T.T.T., Stojaka, K., Ha, P.T., Pham, H.N., Nguyen, X.P., Mukherjee, P., Srikanth, H. and Phan, M.H. (2014) Synthesis, Inductive Heating, and Magnetoimpedance-Based Detection of Multifunctional Fe_3O_4 Nanoconjugates. *Sensors and Actuators B*, **190**, 715-722. https://doi.org/10.1016/j.snb.2013.09.033

[6] Bunge, A., Magerusan, L., Morjan, I., Turcu, R., Borodi, G. and Liebscher, J. (2015) Diazonium Salt-Mediated Synthesis of New Amino, Hydroxy, Propargyl, and Maleinimido-Containing Superparamagnetic Fe@C Nanoparticles as Platforms for

Linking Bio-Entities or Organocatalytic Moieties. *Journal of Nanoparticle Research*, **17**, 379-395. https://doi.org/10.1007/s11051-015-3167-2

[7] Taylor, A., Krupskaya, Y., Costa, S., Oswald, S., Kramer, K., Fussel, S., Klingeler, R., Buchner, B., Borowiak-Palen, E. and Wirth, M.P. (2010) Functionalization of Carbon Encapsulated Iron Nanoparticles. *Journal of Nanoparticle Research*, **12**, 513-519. https://doi.org/10.1007/s11051-009-9773-0

[8] Aguiló-Aguayo, N., Maurizi, L., Galmarini, S., Ollivier-Beuzelin, M.G., Coullerez, G., Bertran, E. and Hofmann, H. (2014) Aqueous Stabilisation of Carbon-Encapsulated Superparamagnetic *α*-Iron Nanoparticles for Biomedical Applications. *Dalton Transactions,* **43**, 13764-13775. https://doi.org/10.1039/C4DT00085D

[9] Davydov, V., Rakhmanina, A., Kireev, I., Alieva, I., Zhironkina, O., Strelkova, O., Dianova, V., Samani, T.D., Mireles, K., Yahia, L.H., Uzbekov, R., Agafonov, V. and Khabashesku, V. (2014) Solid State Synthesis of Carbon-Encapsulated Iron Carbide Nanoparticles and Their Interaction with Living Cells. *Journal of Materials Chemistry B*, **2**, 4250-4261. https://doi.org/10.1039/C3TB21599G

[10] Chaudhary, R.P., Kangasniemi, K., Takahashi, M., Mohanty, S.K., Koymen, A.R. and Bossmann , S.H. (2017) Fe Core-Carbon Shell Nanoparticles as Advanced MRI Contrast Enhancer. *Journal of Functional Biomaterials*, **8**, 46-53. https://doi.org/10.3390/jfb8040046

[11] Peng, H., Alemany, L.B., Margrave, J.L. and Khabashesku, V.N. (2003) Sidewall Carboxylic Acid Functionalization of Single-Walled Carbon Nanotubes. *Journal of the American Chemical Society*, **125**, 15174-15182. https://doi.org/10.1021/ja037746s

[12] Bigall, N.C., Parak, W.J. and Dorfs, D. (2012) Fluorescent, Magnetic and Plasmonic—Hybrid Multifunctional Colloidal Nano Objects. *Nano Today*, **7**, 282-296. https://doi.org/10.1016/j.nantod.2012.06.007

[13] Zhao, Z., Li, W., Dai, Y., Ge, G., Guo, X. and Wang, G. (2015) Carbon Nitride Encapsulated Nanodiamond Hybrid with Improved Catalytic Performance for Clean and Energy-Saving Styrene Production via Direct Dehydrogenation of Ethylbenzene. *ACS Sustainable Chemistry & Engineering,* **3**, 3355-3364. https://doi.org/10.1021/acssuschemeng.5b01032

[14] Ong, W.-J., Tan, L.-L., Ng, Y.H., Yong, S.-T. and Chai, S.-P. (2016) Graphitic Carbon Nitride (g-C$_3$N$_4$)-Based Photocatalysts for Artificial Photosynthesis and Environmental Remediation: Are We a Step Closer to Achieving Sustainability? *Chemical Reviews*, **116**, 7159-7329.

[15] Zimmerman, J.L., Williams, R., Khabashesku, V.N. and Margrave, J.L. (2001) Synthesis of Spherical Carbon Nitride Nanostructures. *Nano Letters*, **1**, 731-734. https://doi.org/10.1021/nl015626h

[16] Zimmerman, J.L., Williams, R., Khabashesku, V.N. and Margrave, J.L. (2001) Preparation of Sphere-Shaped Nanoscale Carbon Nitride Polymer. *Russian Chemical Bulletin*, **50**, 2020-2027. https://doi.org/10.1023/A:1015020511471

[17] Zinin, P.V., Ryabova, A.V., Davydov, V.A., Khabashesku, V., Boritko, S., Sharma, S.K., Pominova, D.V. and Loshenov, V. (2015) Anomalous Fluorescence of the Spherical Carbon Nitride Nanostructures. *Chemical Physics Letters*, **633**, 95-98. https://doi.org/10.1016/j.cplett.2015.05.020

[18] Khabashesku, V.N., Zimmerman, J.L. and Margrave, J.L. (2000) Powder Synthesis and Characterization of Amorphous Carbon Nitride. *Chemistry of Materials*, **12**, 3264-3270. https://doi.org/10.1021/cm000328r

[19] Yuan, Y., Zhang, L., Xing, J., Utama, M.I.B., Lu, X., Du, K., Li, Y., Hu, X., Wang, S., Genc, A., Dunin-Borkowski, R., Arbiol, J. and Xiong, Q. (2015) High-Yield Synthesis and Optical Properties of g-C$_3$N$_4$. *Nanoscale*, **7**, 12343-12350. https://doi.org/10.1039/C5NR02905H

[20] Bystrzejewski, M., Pyrzynska, K., Huczko, A. and Lange, H. (2009) Carbon-Encapsulated Magnetic Nanoparticles as Separable and Mobile Sorbents of Heavy Metal Ions from Aqueous Solutions. *Carbon*, **47**, 1201-1204. https://doi.org/10.1016/j.carbon.2009.01.007

[21] Zhang, L., Jin, Z., Lu, H., Lin, T., Ruan, S., Zhao, X.S. and Zeng, Y.-J. (2018) Improving the Visible-Light Photocatalytic Activity of Graphitic Carbon Nitride by Carbon Black Doping. *ACS Omega*, **3**, 15009-15017. https://doi.org/10.1021/acsomega.8b01933

[22] Wang, H., Zhou, W., Li, P., Tan, X., Liu, Y., Hu, W., Ye, J. and Yu, T. (2018) Enhanced Visible-Light-Driven Hydrogen Production of Carbon Nitride by Band Structure Tuning. *The Journal of Physical Chemistry C*, **122**, 17261-17267. https://doi.org/10.1021/acs.jpcc.8b04224

[23] Rochkind, M., Pasternak, S. and Paz, Y. (2015) Using Dyes for Evaluating Photocatalytic Properties: A Critical Review. *Molecules*, **20**, 88-110. https://doi.org/10.3390/molecules20010088

[24] Duan, S., Han, G., Su, Y., Zhang, X., Liu, Y., Wu, X. and Li, B. (2016) Magnetic Co@g-C$_3$N$_4$ Core-Shells on rGO Sheets for Momentum Transfer with Catalytic Activity toward Continuous-Flow Hydrogen Generation. *Langmuir*, **32**, 6272-6281. https://doi.org/10.1021/acs.langmuir.6b01248

[25] Yu, X., Yang, X. and Li, G. (2018) Magnetically Separable Fe$_2$O$_3$/g-C$_3$N$_4$ Nanocomposites with Cocoon-Like Shape: Magnetic Properties and Photocatalytic Activities. *Journal of Electronic Materials*, **47**, 672-676. https://doi.org/10.1007/s11664-017-5835-8

[26] Xia, X., Zhou, C., Tong, D., Liu, M., Zhang, D., Fang, M. and Yu, W. (2010) Preparation of Magnetic Graphitic Carbon Nitride Nanocomposites. *Materials Letters*, **64**, 2620-2623. https://doi.org/10.1016/j.matlet.2010.08.064

[27] Wang, Y., Wang, X. and Antonietti, M. (2012) Polymeric Graphitic Carbon Nitride as a Heterogeneous Organocatalyst: From Photochemistry to Multipurpose Catalysis to Sustainable Chemistry. *Angewandte Chemie International Edition*, **51**, 68-89. https://doi.org/10.1002/anie.201101182

[28] Yan, S.C., Li, Z.S. and Zou, Z.G. (2009) Photodegradation Performance of g-C$_3$N$_4$ Fabricated by Directly Heating Melamine. *Langmuir*, **25**, 10397-10401. https://doi.org/10.1021/la900923z

[29] Baig, R.B.N., Verma, S., Varma, R.S. and Nadagouda, M.N. (2016) Magnetic Fe@g-C$_3$N$_4$: A Photoactive Catalyst for the Hydrogenation of Alkenes and Alkynes. *ACS Sustainable Chemistry & Engineering*, **4**, 1661-1664. https://doi.org/10.1021/acssuschemeng.5b01610

[30] Chen, Z., Zhang, J., Zheng, S., Ding, J., Sun, J., Dong, M., Abbas, M., Chen, Y., Jiang, Z. and Chen, J. (2018) The Texture Evolution of g-C$_3$N$_4$ Nanosheets Supported Fe Catalyst During Fischer-Tropsch Synthesis. *Molecular Catalysis*, **444**, 90-99. https://doi.org/10.1016/j.molcata.2016.12.011

[31] Beveridge, J.S., Stephens, J.R. and Williams, M.E. (2011) The Use of Magnetic Nanoparticles in Analytical Chemistry. *Annual Review of Analytical Chemistry*, **4**, 251-273. https://doi.org/10.1146/annurev-anchem-061010-114041